Formation of dysprosium carbide on the graphite (0001) surface

Ann Lii-Rosales,[1,2] Yinghui Zhou,[1,*] Mark Wallingford,[1] Cai-Zhuang Wang,[1,3] Michael C. Tringides,[1,3] and P. A. Thiel[1,2,4,†]

[1]*The Ames Laboratory, Ames, Iowa 50011, USA*

[2]*Department of Chemistry, Iowa State University, Ames, Iowa 50011, USA*

[3]*Department of Physics & Astronomy, Iowa State University, Ames, Iowa 50011, USA*

[4]*Department of Materials Science & Engineering, Iowa State University, Ames, Iowa 50011, USA*

(Received 26 February 2017; published 12 July 2017)

Using scanning tunneling microscopy, we characterize a surface carbide that forms when Dy is deposited on the basal plane of graphite. To form carbide islands on terraces, Dy is first deposited at 650–800 K, which forms large metallic islands. Upon annealing at 1000 K, these clusters convert to carbide. Deposition directly at 1000 K is ineffective because nucleation on terraces is inhibited. Reaction is signaled by the fact that each carbide cluster is partially or totally surrounded by an etch pit. The etch pit is one carbon layer deep for most carbide clusters. Carbide clusters are also identifiable by striations on their surfaces. Based on mass balance, and assuming that only the surface layer of carbon is involved in the reaction, the carbide has stoichiometry Dy_2C. This is Dy-rich compared with the most common bulk carbide DyC_2, which may reflect limited surface carbon transport to the carbide.

DOI: 10.1103/PhysRevMaterials.1.026002

I. INTRODUCTION

There is currently significant interest in systems wherein magnetic metals interact with graphitic surfaces, from single-layer graphene to few-layer graphene to bulk graphite. Such systems hold promise for designing and controlling magnetic properties at the nanoscale, and for protecting magnetic materials that would otherwise degrade via oxidation [1–4]. However, reaction of the metal to form a carbide can also be detrimental. It is thus important to understand the conditions under which metal carbide forms, and how to identify it. This paper addresses that topic for Dy interacting with the basal plane of graphite, where graphite is chosen as a tractable prototype for carbon-rich surfaces, and Dy is selected because it is one of the rare earths, which have notably high magnetic moments.

It is known that reactions of Dy and other rare earths with *bulk* graphite can produce both intercalation compounds and carbides. Their formation requires elevated temperatures. Bulk intercalation and carbide formation compete above 700 K [5]. It is thus reasonable to expect that elevated temperature is necessary to form a surface carbide.

Several previous *surface* studies, dealing with the rare earths Gd, Dy, and La on graphite, are relevant to this work [6–8]. After depositing multilayers (tens to hundreds of monolayers) of each rare earth (R) on graphite at room temperature, annealing to elevated temperature produced a carbide identified as RC_2, followed by a disordered carbon layer atop the carbide at higher temperature, and a graphene sheet at still higher temperature. The conclusions were drawn from x-ray photoelectron and Auger electron spectroscopies, and from low-energy electron diffraction data. The present study differs in several ways. In particular, it deals with lower coverages of metal, and it employs STM.

In other relevant prior work, we have shown that deposition of Dy at room temperature, up to a few monolayers, produces Dy islands on terraces [9]. The islands are irregularly shaped with a base that is three layers high. Upper levels on the islands are populated in clearly resolved single-layer increments. A moiré pattern is often present atop the three-layer rafts. Density functional theory calculations show that a single Dy atom interacts rather strongly with graphite, having an adsorption energy of −1.90 eV. The difference in adsorption energies between various sites is small, only 7 meV. The number density of Dy islands at 300 K is quantitatively consistent with a diffusion barrier derived from the difference in adsorption energies, and experimental parameters [9].

II. EXPERIMENTAL DETAILS

All experiments were performed in an ultrahigh vacuum (UHV) chamber with a base pressure of 3×10^{-11} mbar. Each clean graphite surface was prepared from a sample of highly oriented pyrolytic graphite (HOPG, ZYB grade) via tape cleavage in air followed by transfer into the UHV chamber, where it was outgassed at 800 K for 20 min to remove contaminants. HOPG has a high degree of perfection along the [0001] direction (perpendicular to the graphene sheets) but typically contains micron-size rotational domains within the sheets [10]. After cleavage, surface cleanliness was checked using an Omicron variable temperature scanning tunneling microscope and all imaging was performed at 300 K. Once deemed clean, Dy was deposited onto the pristine HOPG at various sample temperatures via physical vapor deposition using a Mantis QUAD-EV-C Mini *e*-beam evaporator. The Dy flux F ranged from 0.042 to 0.24 ML/s.

Sample heating was achieved using an Omicron dual filament *e*-beam heater. Temperature measurements below 900 K were based on a calibration curve established by calibrating the power from the *e*-beam heater to the reading from a remote thermocouple that was brought into direct contact with the graphite surface. Temperatures of 900 K and above were measured using a Wahl Heat Spy infrared thermometer and an emissivity for graphite of 1.0.

For Dy deposition at 300 K, STM imaging was conducted at +1.0 to +1.6 V tip bias and 0.25 to 0.27 nA tunneling current. For deposition temperatures $T_{dep} \geqslant 650$ K, scanning

*Present address: Department of Physics, Xiamen University, Xiamen 361005, China.

†thiel@ameslab.gov

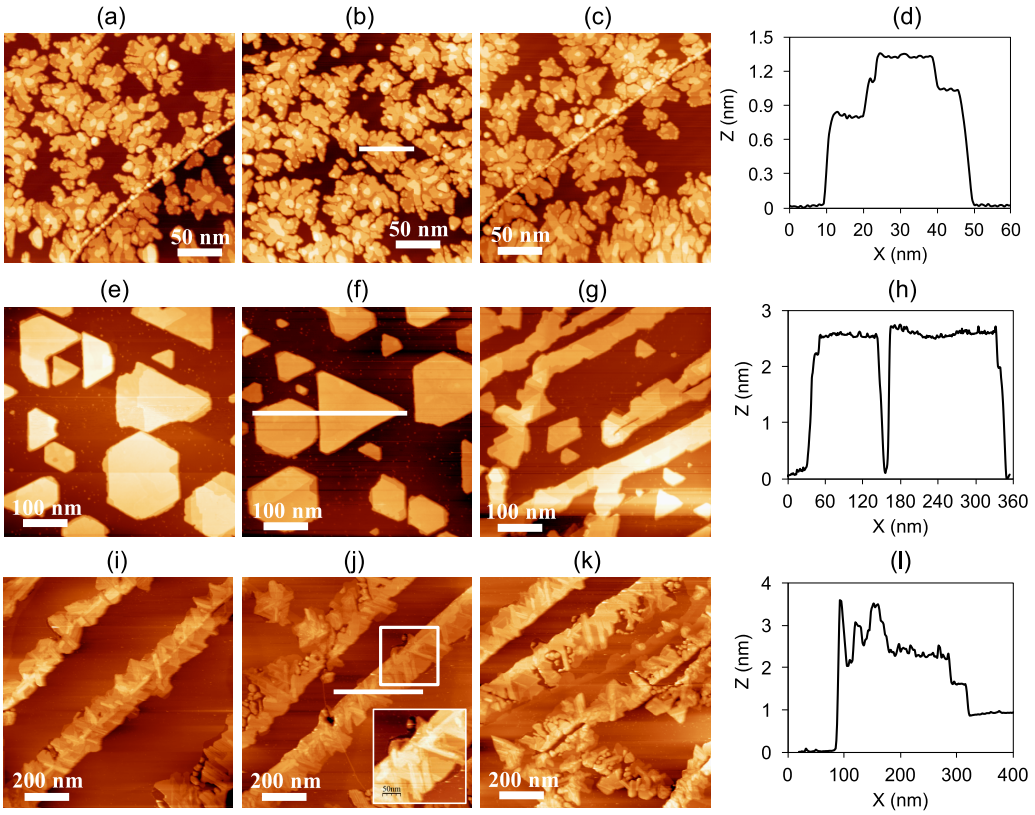

FIG. 1. Representative STM images of Dy after deposition on pristine graphite at various temperatures, and line profiles associated with the horizontal bars in the STM images. (a)–(d) 300 K and 2.55 ± 0.17 ML. (e)–(h) 650 K and 2.50 ± 0.51 ML. (g) An area that is dense with graphite step edges. (i)–(l) 1000 K; all areas are dense with graphite step edges. Inset in (j) shows enlargement of the white square on the step.

was carried out at +1.3 to +4.3 V tip bias and 0.15 to 0.28 nA tunneling current. The STM tip was etched electrochemically from a W wire. All STM images were planed and analyzed using WSxM software [11]. Coverages were determined by flooding images and analyzing Dy island volumes. We define 1 monolayer (ML) as the amount of Dy required to completely cover the graphite surface to a depth of one atomic layer, assuming that the density of Dy is the same as that in a close-packed plane of bulk Dy. Flux was calculated from coverage and deposition time.

Previously, we showed that nucleation of Cu islands on graphite was sensitive to the presence of Cu ions that were generated by this same *e*-beam evaporator [12]. Although they were only a tiny fraction of the total Cu flux—0.05%—the ions produced defect sites for heterogeneous nucleation on the graphite terraces. In the present study we were not concerned with nucleation kinetics or mechanisms, and we used the evaporator under conditions where Dy ions were likely present.

III. RESULTS

A. Deposition at various temperatures

We begin by surveying the characteristics of islands formed after Dy deposition at various temperatures $T_{dep} = 300$ to 1000 K. This lays the groundwork for distinguishing various forms of adsorbed Dy from the carbide.

At 300 K, deposition produces islands of metallic Dy that are close packed and commensurate with the graphite substrate [9]. Examples are shown in Figs. 1(a)–1(c). The three-layer base is clearly evident as the lowest level in the line profile of Fig. 1(d). Step edges of the graphite substrate are decorated with Dy, but not more heavily than the surrounding terraces, as seen from the steps that cut diagonally across Figs. 1(a) and 1(c).

At higher temperatures, islands on terraces are much different. Deposition on graphite at 650–800 K produces tall, compact three-dimensional islands that are faceted in the shapes of triangles, truncated triangles, or hexagons, as seen in Figs. 1(e) and 1(f). By analogy with our previous analysis of island shapes of Dy on graphene [13], this mixture of geometric shapes suggests a mixture of fcc and hcp metallic growth, with the close-packed planes of Dy parallel to the graphite surface. At comparable coverage, the islands produced at 650–800 K are significantly taller than those observed at 300 K, as illustrated by comparing the line profiles in Fig. 1(d) with Fig. 1(h). Also, the graphite step edges are more heavily decorated at 650–800 K than at 300 K. Figure 1(g) shows an area that is dense in step edges. Notably, the graphite steps are covered by continuous, flat strips of Dy.

At 1000 K, Dy rarely forms islands on terraces. Instead, almost all of the Dy is located at step edges. These step edges have a distinctive appearance. Compared with the steps prepared at 650–800 K, the decoration is irregular and rough. Furthermore, one often sees striations atop the clumps, as shown by the inset to Fig. 1(j). Based on material presented in the following section, the striations and roughness lead us

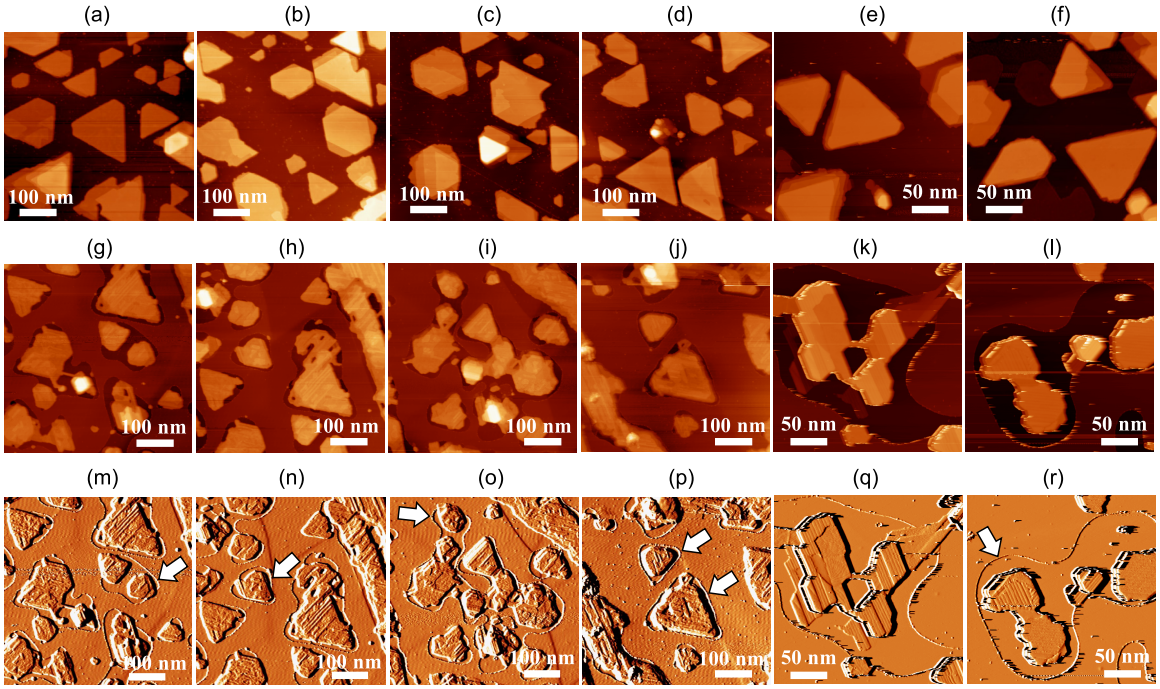

FIG. 2. STM images of Dy deposited at 650 K on pristine graphite (a)–(f), Dy carbide islands that form after annealing at 1000 K for 10 min (g)–(l), and their respective derivatized images (m)–(r). These images are obtained in two separate experiments, represented in (a)–(d), (g)–(j), and (m)–(p) and (e) and (f), (k) and (l), and (q) and (r), respectively. Note that images in the second experiment are at twofold higher magnification.

to identify these step features as Dy carbide. Evidence for carbon consumption is not evident at the steps, because the steps presumably recede as carbon is consumed. However, the situation is different when carbide forms on the terraces, as discussed below.

B. Deposition followed by annealing

The previous section showed that it is not possible to form significant amounts of carbide on the terraces by varying the deposition temperature. Either the temperature is too low to initiate the reaction ($T_{\mathrm{dep}} < 800$ K), or the temperature is too high to foster nucleation on terraces ($T_{\mathrm{dep}} = 1000$ K). We therefore choose deposition conditions that serve to create large islands of metallic Dy on terraces, then heat the surface in order to initiate reaction.

To this end, compact 3D dysprosium islands were formed by deposition at 650 K, then annealed at 1000 K for 10 min. Figures 2(a)–2(f) shows islands after deposition, and lower panels show islands after annealing. In three similar experiments, the island density decreased by only $15 \pm 6\%$ after annealing for 10 min, indicating that annealing causes limited coarsening.

Several changes in island morphology are produced by annealing, as shown in Fig. 2. First, island footprints become more irregular than before (middle row in Fig. 2). Second, the island tops are much rougher than before annealing. They often exhibit long and thin striations on their tops. These striations are especially noticeable in the derivatized images (bottom row in Fig. 2). Third, around each island, or collection of islands, there is a depressed ring. Rings from different islands can merge. The arrows in Figs. 2(m), 2(o), and 2(r) point to examples. Furthermore, for nonmerged rings, the ring shape resembles the approximate shape of the island it encloses. The arrows in Figs. 2(n) and 2(p) mark examples. The height of the carbide islands is not uniform, ranging from 2 to 3 nm in our experiments. The edges and other features in the carbide islands often make angles of 120° or 60°, which could be a vestige of the original metallic island shape.

Additional annealing at 1000 K for 30 or 60 min does not promote noticeable growth of the depressions in either vertical or lateral directions. There are also no noticeable changes in island morphology or island density. Regarding island density, in one experiment, the island density after 10 and 30 min annealing is $(3.5 \pm 0.5) \times 10^{-5}$ and $(4.0 \pm 1.0) \times 10^{-5}$ nm^{-2}, respectively. In another experiment, the island density after 10 and 60 min annealing is $(5.1 \pm 0.4) \times 10^{-5}$ and $(5.1 \pm 0.3) \times 10^{-5}$ nm^{-2}, respectively. Hence, island densities are unchanged by longer annealing times, reflecting high thermal stability of the rough islands at 1000 K.

The depressed ring is 0.34 ± 0.01 nm deep (averaged over 60 rings). Depths are analyzed via height histograms as illustrated in Fig. 3. The depth is, within error, the same as the expected interplanar separation between graphene sheets in bulk graphite (0.335 nm). For 90% of the islands, the surrounding rings are one C layer deep, meaning that multiple layers are not involved. In the remaining 10% of islands, we see small regions in the ring that are two C layers deep. Examples of the latter are shown in Fig. 4. Furthermore, the pit edges have protruding rims. These are especially evident in the line profiles of Fig. 4. These protruding rims have been observed and studied by Atamny *et al.* on clean graphite step edges [14], where they have been attributed to tip-induced deformation of the top C sheet at the step edge.

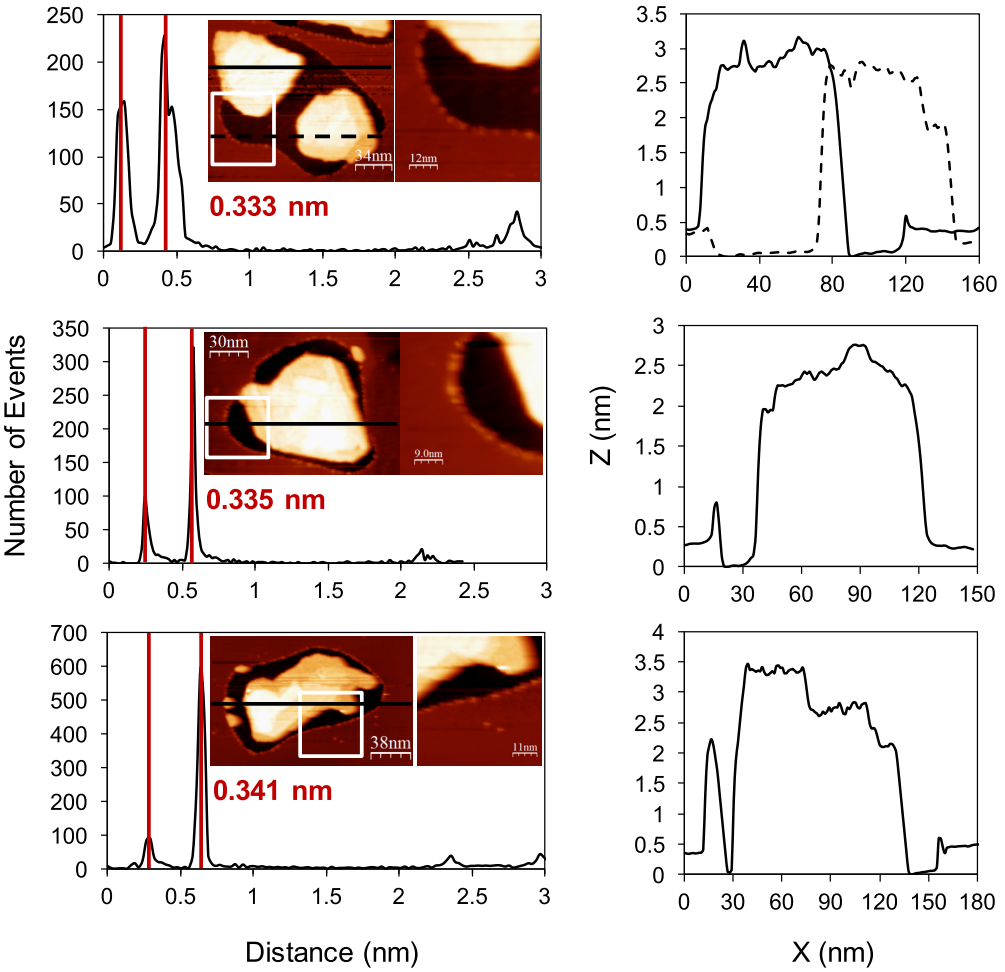

FIG. 3. Height histograms showing the depth of rings around islands after annealing at 1000 K. Height histograms are generated from the zoomed-in areas of the ring and island as shown by the white boxes. The two peaks marked by red lines correspond to one layer of graphene, which is 0.335 nm in bulk graphite. Line profiles of carbide islands along the black lines are shown in the right panel.

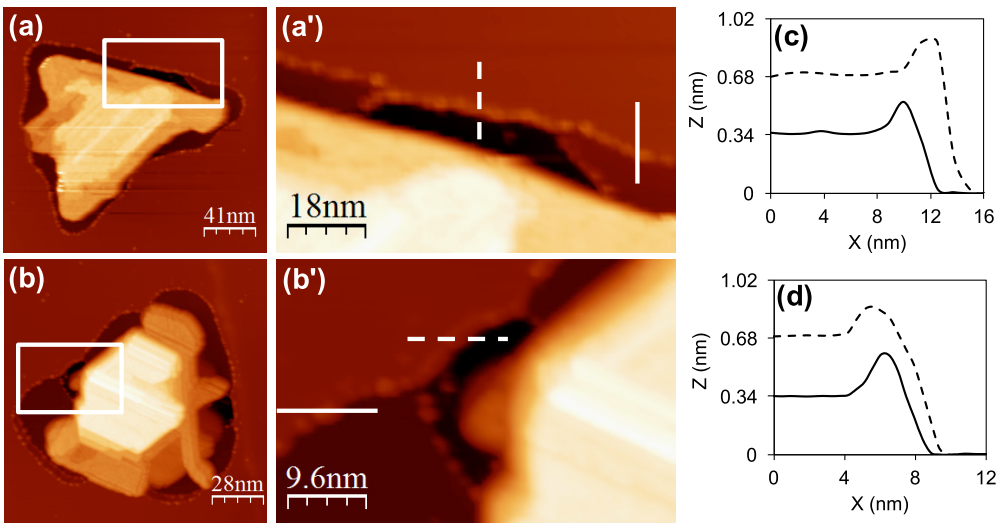

FIG. 4. (a) and (b) Dy carbide islands with small regions that are two C layers deep in the depressed ring as outlined by white rectangles. (a′) and (b′) Enlargement of the areas in the white rectangles, with line profiles (c) and (d) indicating a single C layer (solid lines) and double C layers (dashed lines). Regions such as these are observed around a small fraction of carbide islands (∼10%).

TABLE I. Carbon ratios, calculated from experimental data, for all four forms of bulk Dy carbide. The C ratio denotes the ratio of C from graphite erosion, both in the etch pit and in a single layer at the base of the island, to C in the carbide island for a given stoichiometry. It equals 1 for a perfect match. For this analysis, 12 islands are used. To be included in the analysis, islands are required to have at least 80% of the perimeter in contact with the etch pit.

Dy_xC_y	DyC_2	Dy_2C_3	Dy_2C	Dy_3C
C ratio	0.38 ± 0.03	0.43 ± 0.04	1.21 ± 0.10	2.41 ± 0.21

We identify the rings as etch pits where carbon is consumed by reaction with the inner Dy island. Reaction is also supported by the morphology changes in the islands themselves. The fact that etch pits are consistently one layer deep suggests that the reaction interface is limited to a single layer at the base of the island. Assuming that this is the case, we have undertaken an analysis of the carbon mass balance, to determine the type of carbide that forms. For this analysis, we only consider islands where at least 80% of the perimeter is in contact with the etch pit, as this ensures a more complete reaction.

There are four known forms of *bulk* dysprosium carbide: DyC_2, Dy_2C_3, Dy_2C, and Dy_3C [15]. In order to find which bulk stoichiometry is most compatible with our experimental data, we calculate the amount of carbon consumed from the etch pit, and from a single layer of carbon beneath the area of the island. We then calculate the amount of carbon in the carbide island for a given stoichiometry, based on its volume. The ratio of these two numbers is 1 for a perfect match. Results are shown in Table I, where best agreement is obtained for Dy_2C. The ratio obtained, 1.21 ± 0.10, is slightly higher than the ideal of 1.0. This deviation could be due to the presence of Dy_3C or unreacted Dy metal, either of which would make the island somewhat more Dy rich than expected for Dy_2C alone.

Height histograms of metal and carbide islands are shown for a representative experiment in Fig. 5. We have chosen the bottom of the etch pit as the base of the island when calculating carbide height, whereas the base is the top graphitic layer for metal island height. Then the average height is 2.30 ± 0.33 nm for the metal, and 2.81 ± 0.33 nm for the carbide. The carbide is 22% (0.51 nm) higher than the metal, but this difference falls within the standard deviations. We conclude that the carbide islands are only slightly, if at all, taller than the metal precursor islands.

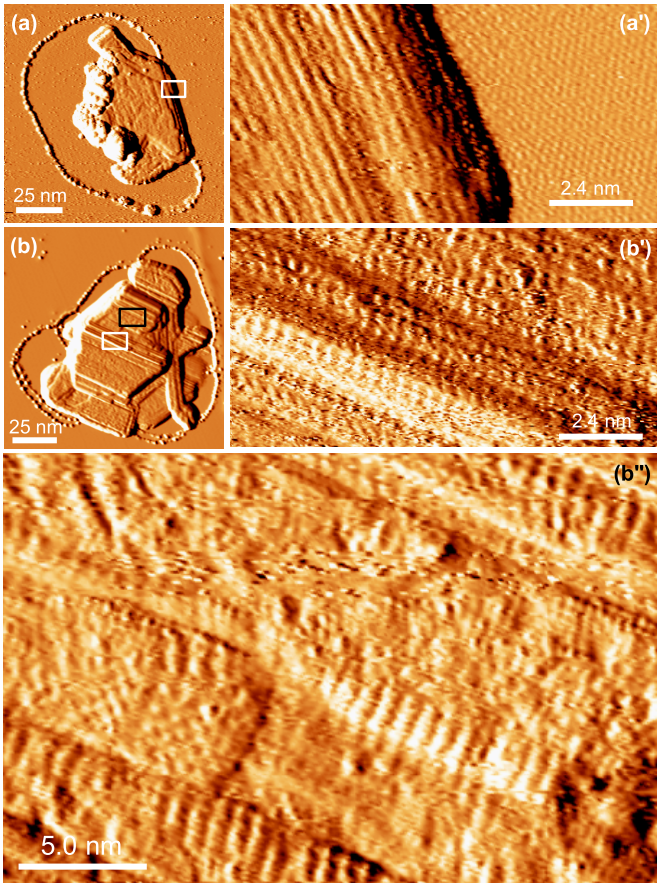

FIG. 6. Derivatized STM images of carbide islands. (a) A carbide island at low magnification. The white box is enlarged and shown in (a′) to reveal the fine structure. (b) Another carbide island. The white box is enlarged in (b′) and the black box in (b″).

C. Fine structure of carbide islands

At high magnification, carbide islands exhibit a rich fine structure. Examples are shown in Fig. 6. The striations that are visible at lower magnification (Fig. 2) form a background to this fine structure. It usually consists of rows that are parallel to the larger striations [cf. Fig. 6(a′)]. The fine structure is very different from the atomic structure within the graphite surface, which is shown on the right side of Fig. 6(a′). The rows in Fig. 6(a′) are separated by 0.37 ± 0.01 nm. In other images, regular features can be resolved along the rows, at a separation

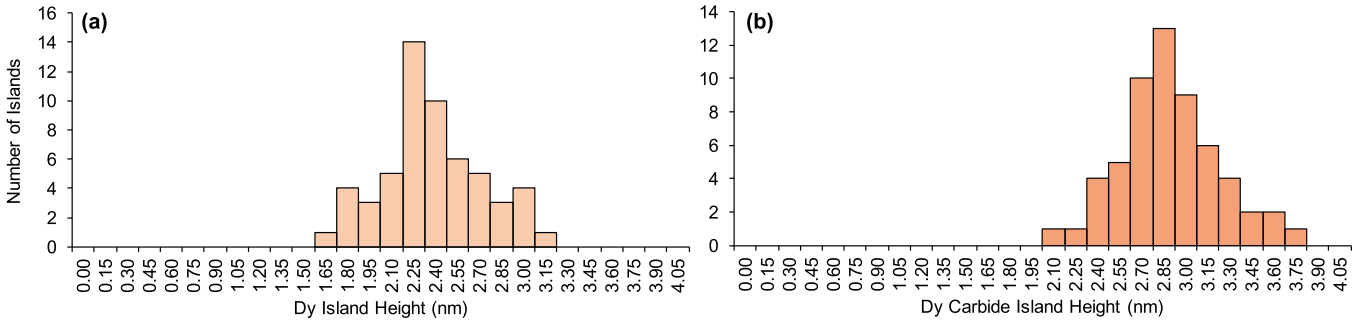

FIG. 5. Height histograms of (a) Dy metal islands (56 islands, average height is 2.30 ± 0.33 nm) and (b) Dy carbide islands (58 islands, average height is 2.81 ± 0.33 nm). Annealing time is 70 min total for this experiment. Bin size for both histograms is 0.15 nm.

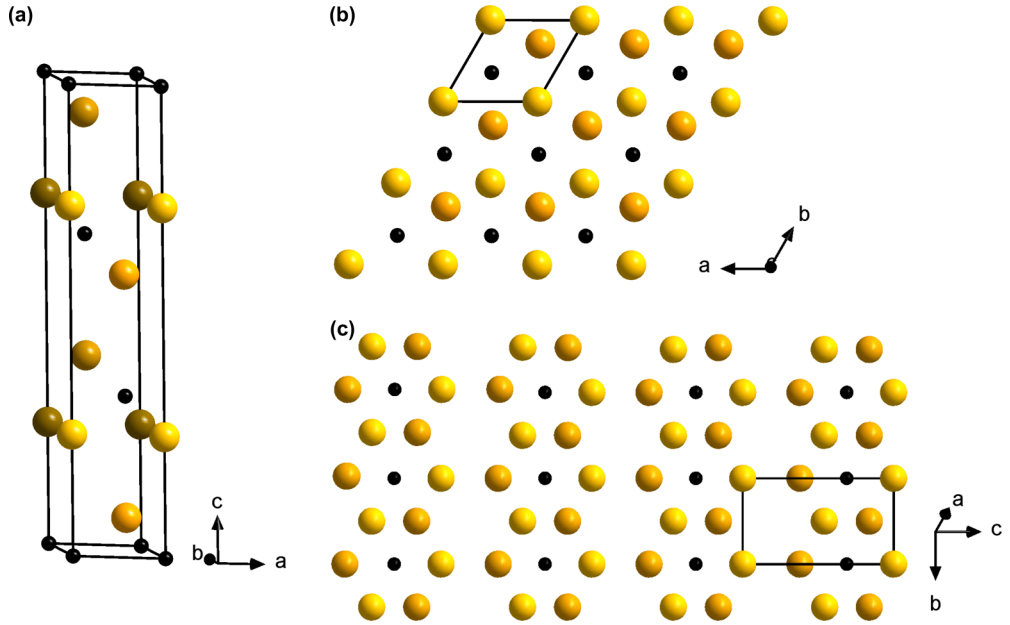

FIG. 7. Bulk structure and two bulk terminations of Dy_2C. C atoms are shown as black dots. Dy atoms are shown in multicolor, with atoms closest to the viewer colored bright yellow, and deeper atoms colored progressively darker. (a) Bulk unit cell. (b) Dy-terminated (001) surface. Black rhombus is the surface unit cell. (c) Dy-terminated $(1/2,0,\bar{2})$ surface, which exhibits a row structure parallel to the *b* axis. Black rectangle is the surface unit cell.

of 0.39 ± 0.01 nm or by twice this value, 0.79 ± 0.02 nm. In other areas, like Fig. 6(b′) which is an enlargement of the features in the black box in Fig. 6(b), the fine structure is irregular. This variation indicates that the carbide islands are not perfect single crystals, but the alignment of rows and striations suggests that individual carbide grains align preferentially along a common axis that lies in the surface plane.

Dy_2C belongs to the trigonal crystal system and has lattice constants $a = b = 0.3584$ nm and $c = 1.789$ nm. The bulk atomic structure is shown in Fig. 7(a). Since surface stability usually correlates with atomic density, a likely candidate for a bulk termination would be the dense (001) surface, as illustrated in Fig. 7(b) for a Dy termination. However, this surface has hexagonal symmetry and is intrinsically incompatible with rows. Another candidate is the $(1/2, 0,\bar{2})$ surface shown in Fig. 7(c). This surface has a row structure, while still exhibiting a high density of Dy atoms [99.6% of the (001) surface]. However, the inter-row separation is 0.63 nm, incompatible with the observed value of 0.37 nm.

We have considered other bulk terminations of Dy_2C as well, but have not found any that fits the experimental observations completely. We conclude that the surface of the carbide is probably reconstructed, i.e., it does not represent a bulk termination.

IV. DISCUSSION

The trademark features of the carbide in STM are the etch pit, the striations, and a footprint that is irregular and rounded compared to the faceted metallic islands. Furthermore, the height is nonuniform, ranging from 2 to 3 nm under our experimental conditions. The striations (resolved at low magnification) form background for a fine structure (resolved at higher magnification) that most often consists of rows of features wherein the rows lie parallel to the striations. Collectively, these features clearly distinguish the carbide from Dy islands, formed either at 300 K or at 650–800 K. Neither form of metallic Dy has etch pits or striations. Furthermore, the vertical profile of the carbide distinguishes it from the islands formed at 300 K, where the three-layer base is strongly evident.

In our experiments, good conditions for producing surface carbide are to deposit Dy on pristine graphite at 650–800 K, thereby producing large faceted islands of Dy metal on the terraces, then anneal to 1000 K. The islands largely retain their identity during the transition from metal to carbide, based on the limited change in island number density (15%). By contrast, direct deposition at 1000 K produces carbide mainly at step edges. Nucleation on terraces is obviously inhibited when Dy is deposited at 1000 K, which is reasonably attributed to a higher Dy diffusion coefficient, larger critical size, and/or less-efficient trapping at terrace defect sites. This leads to preferential growth and reaction at steps.

The bulk structure of Dy_2C (Fig. 7) consists of planes of hexagonally close-packed Dy atoms with density nearly the same as that of bulk Dy metal (equal within 0.5%), and planes of C atoms. Pairs of Dy planes alternate with single C planes. Thus, in order to form this carbide, carbon must simply insert in alternating spaces between Dy sheets, causing only slight change in lattice positions of Dy atoms in the (001) planes. [A similar argument can be made for $(1/2,0,\bar{2})$ planes, but with insertion of C between every pair of Dy sheets.] This would account for the observation that carbide islands often have triangular or hexagonal footprints reminiscent of the original Dy clusters (Fig. 2)—they can retain their macroscopic shape during the transformation. Furthermore, the island heights increase only slightly during the transformation. This is consistent with expectation based on crystallographic data for bulk Dy metal and bulk Dy_2C.

From that data, the spacing between close-packed layers of Dy is (on average) only 7% larger in the carbide than in the metal.

The data lead us to suggest the following model for metal-to-carbide transformation. First, reaction begins at the base of metal islands, at the interface between Dy and graphite. The reaction serves to create or enhance defects in the carbon layer beneath the Dy island. These defects grow laterally within the carbon layer as reaction proceeds, because carbon at the edges of the defects has a higher chemical potential than fully sp^2-coordinated carbon in the graphite layer beneath. The defects continue to grow outward even beyond the base of the metal island, creating monolayer etch pits.

Within the metal, carbon atoms must diffuse. Data for C diffusion in Dy are unavailable to our knowledge, but C diffusion in bulk Fe has been studied extensively. It is known that interstitial diffusion of C in Fe is very fast—at 800 K the net diffusion length is at least 1 μm [16]. Extrapolating to metallic Dy, we suggest that diffusion of carbon atoms at 1000 K is facile. Thus they can easily arrange as sheets between pairs of close-packed planes of Dy metal, forming Dy_2C.

Based on mass balance of carbon, the carbide is mainly Dy_2C. A more carbon-rich phase DyC_2 is most common among the bulk carbides. It is therefore somewhat surprising that DyC_2 does not form in our system, given the essentially infinite reservoir of carbon. We hypothesize that the supply of carbon is limited, perhaps by carbon detachment and diffusion from the etch pit.

Comparing our work with prior work, a study of carbide formation at the Dy-graphite surface assigned the carbide as DyC_2 [6]. However, the annealing temperature of 1200 K was higher than that used in the present work, 1000 K. At our temperature, the Dy_2C islands are stable against long annealing, i.e., there is no evidence of transformation into DyC_2 over time. However, it is possible that different carbides form at different temperatures, which would be an interesting topic for future work. Also, we see no evidence for a graphene layer covering the carbide, as reported previously [7,8], but that too may be attributable to different annealing temperatures. The graphene overlayer was observed after annealing at 1400 K, a much higher temperature than used in our work.

V. CONCLUSIONS

Formation of surface carbide is readily identifiable using STM, in the Dy/graphite system. The etch pit is evidence for consumption of carbon. Changes in the island morphology, especially the surface striations and the irregular, somewhat-rounded footprint, accompany the appearance of the etch pit. Together, these features clearly distinguish the carbide from Dy islands. An effective strategy for forming the carbide on terraces is to deposit Dy at 650–800 K, then anneal at 1000 K. Deposition directly at 1000 K causes the carbide to grow almost exclusively at graphite step edges. The carbide is Dy_2C, based on mass balance and on the assumption that reaction is limited to a single carbon layer. The fine structure of the islands is not compatible with any dense bulk termination of Dy_2C, suggesting that the carbide surface is reconstructed.

ACKNOWLEDGMENTS

This work was supported by the Division of Materials Sciences, Basic Energy Sciences, U.S. Department of Energy (DOE). The research was performed at Ames Laboratory, which is operated for the U.S. DOE by Iowa State University under Contract No. DE-AC02-07CH11358. Y.Z.'s participation was supported by the China Scholarship Council. We thank Gordon J. Miller for providing insight into the structure of bulk Dy_2C.

The data presented in this paper are available at DOI:10.17039/ameslab.dmse.2017.DS7/1364117.

[1] V.-V. Chi, K.-B. Zoukaa, Y. Hongxin, C. Johann, V. Jan, P. Stefania, B.-G. Pascale, C. Mairbek, R. Laurent, G. Valérie, D. Philippe, S. Violaine, and F. Olivier, New J. Phys. **12**, 103040 (2010).

[2] S. M. Binz, M. Hupalo, X. J. Liu, C. Z. Wang, W.-C. Lu, P. A. Thiel, K. M. Ho, E. H. Conrad, and M. C. Tringides, Phys. Rev. Lett. **109**, 026103 (2012).

[3] L. H. de Lima, R. Landers, and A. de Siervo, Chem. Mater. **26**, 4172 (2014).

[4] W. Zhou, J. Zhou, Y. Zhou, J. Lu, K. Zhou, L. Yang, Z. Tang, L. Li, and S. Chen, Chem. Mater. **27**, 2026 (2015).

[5] R. Hagiwara, M. Ito, and Y. Ito, Carbon **34**, 1591 (1996).

[6] S. A. Gorovikov, A. M. Shikin, G. V. Prudnikova, V. K. Adamchuk, S. L. Molodtsov, C. Laubschat, and A. M. Ionov, Surf. Sci. **474**, 98 (2001).

[7] A. M. Shikin, V. K. Adamchuk, S. Siebentritt, K. H. Rieder, S. L. Molodtsov, and C. Laubschat, Phys. Rev. B **61**, 7752 (2000).

[8] A. Vyatkin, S. Gorovikov, A. Shikin, V. Adamchuk, J. Avila, M.-C. Asensio, and S. Molodtsov, Phys. Low-Dim. Struct. **12**, 339 (1995).

[9] E. Kwolek, H. Lei, A. Lii-Rosales, M. Wallingford, Y. Zhou, C.-Z. Wang, M. C. Tringides, J. W. Evans, and P. A. Thiel, J. Chem. Phys. **145**, 211902 (2016).

[10] N. Ferralis, K. Pussi, S. E. Finberg, J. Smerdon, M. Lindroos, R. McGrath, and R. D. Diehl, Phys. Rev. B **70**, 245407 (2004).

[11] I. Horcas, R. Fernández, J. M. Gómez-Rodríguez, J. Colchero, J. Gómez-Herrero, and A. M. Baro, Rev. Sci. Instrum. **78**, 013705 (2007).

[12] D. Appy, H. Lei, Y. Han, C.-Z. Wang, M. C. Tringides, D. Shao, E. J. Kwolek, J. W. Evans, and P. A. Thiel, Phys. Rev. B **90**, 195406 (2014).

[13] M. T. Hershberger, M. Hupalo, P. A. Thiel, and M. C. Tringides, J. Phys.: Condens. Matter **25**, 225005 (2013).

[14] F. Atamny, T. F. Fässler, A. Baiker, and R. Schlögl, Appl. Phys. A **71**, 441 (2000).

[15] G.-Y. Adachi, N. Imanaka, and F. Zhang, *Handbook on the Physics and Chemistry of Rare Earths* (Elsevier Science Publishers, B.V., Netherlands, 1991), Vol. 15, p. 61.

[16] T. Heumann, *Diffusion in Metallen: Grundlagen, Theorie, Vorgänge in Reinmetallen und Legierungen* (Springer, Berlin, 1992).